ACS APPLIED MATERIALS & INTERFACES

Research Article

www.acsami.org

MOF-Derived Cobalt-Doped ZnO@C Composites as a High-Performance Anode Material for Lithium-Ion Batteries

Hongyun Yue,*[,†,‡,§] Zhenpu Shi,[†] Qiuxian Wang,[†] Zhaoxia Cao,[†,‡,§] Hongyu Dong,[†,‡,§] Yun Qiao,[†,‡,§] Yanhong Yin,[†,‡,§] and Shuting Yang*[,†,‡,§]

[†]School of Chemistry and Chemical Engineering, [‡]Engineering Technology Research Center of Motive Power and Key Materials, and [§]Collaborative Innovation Center of Henan Province for Motive Power and Key Materials, Henan Normal University, Xinxiang Henan 453007, P. R. China

Supporting Information

ABSTRACT: Cobalt (Co)-doped MOF-5s (Co-MOF-5s) were first synthesized by a secondary growth method, followed by a heat treatment to yield Co-doped ZnO coated with carbon (CZO@C). Compared with carbon-coated ZnO (ZnO@C), the doping of Co increased the graphitization degree of the carbon on the surface of CZO@C nanoparticles and enhanced the conductivity of the material. The electrochemical properties of the materials were characterized by galvanostatic discharge/charge tests. It was found that the as-synthesized CZO@C composites enabled a reversible capacity of 725 mA h g^{-1} up to the 50th cycle at a current density of 100 mA g^{-1}, which was higher than that of ZnO@C composites (335 mA h g^{-1}).

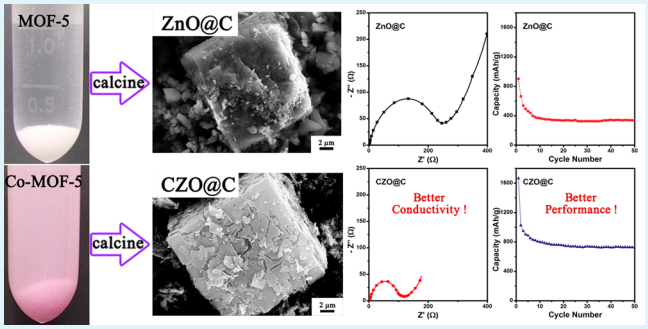

KEYWORDS: *zinc oxide, metal−organic frameworks, cobalt doping, anode material, lithium-ion batteries*

1. INTRODUCTION

Metal−organic frameworks (MOFs) are a class of rapidly growing adsorbent materials that have high surface area with high porosity.[1−3] The structure of MOFs can be designed according to the target properties by careful selection of metal centers and different functional linkers. Until now, MOFs have been studied in many fields because of their excellent properties, such as gas storage and separation,[4] sensing or recognition,[5] catalysis,[6] electrochemistry,[7] and so on. Presently, the application of MOFs in electrochemistry is still in its infancy, and they are most commonly used as precursors for the synthesis of nano metal oxides or nanoporous carbon.[8] The ZnO quantum dots and ZnO@C composites have been obtained by simple heat treatments of MOF-5 and used as photocatalysts or anode materials in lithium-ion batteries (LIBs).[9,10]

LIBs, a fast-developing technology area in electric energy storage, are promising power sources for a wide range of portable electronic devices. The increasing demand for high-performance LIBs compels people to explore novel electrode materials with high capacity and long life.[11,12] A variety of materials can be used in LIBs, such as ZnO, which has a much higher theoretical capacity of 978 mA h g^{-1} than that of graphite (372 mA h g^{-1}).[13,14] Compared with the other metal oxides, ZnO undergoes an undesirable large volume expansion during cycling that leads to a significant falloff in capacity, and the common way to overcome the volume expansion is to decrease the particle size of ZnO.[15] Another disadvantage of ZnO is the poor electronic conduction.[16,17] In order to conquer that, coating ZnO with carbon has been carried out by many previous researches.[18−20]

In this work, the cobalt (Co)-doped MOF-5s (Co-MOF-5s) were first synthesized by a secondary growth method. CZO@C nanoparticles were obtained via heat treatment of Co-MOF-5s under a nitrogen atmosphere. The doping of Co enhanced the conductive of ZnO nanoparticles and increased the graphitization degree of the carbon coated on the nanoparticles. The higher graphitization degree was beneficial to the electronic conduction of the whole nanocomposites, which would quicken the charge-transfer rate at the interface between active material and electrolyte and thus improve the cycle stability.

2. EXPERIMENTAL SECTION

Material Synthesis. Zinc nitrate hexahydrate (6.0 mmol) and terephthalic acid (2.0 mmol) were dissolved in 60 mL of *N*,*N*-dimethylformamide in an autoclave. The reaction mixture was heated at 120 °C in an oven to yield cubic crystals of MOF-5. Different amounts of cobalt nitrate hexahydrate (0.5, 1.0, 2.0, and 3.0 wt %) were added into the reaction system after the autoclave was cooled to room temperature. The mixture was stirred for 12 h in sealed surroundings, and the reaction vessels were then heated again at 120 °C for 24 h to yield Co-MOF-5 crystals. The obtained samples were

Received: July 17, 2014
Accepted: September 15, 2014
Published: September 15, 2014

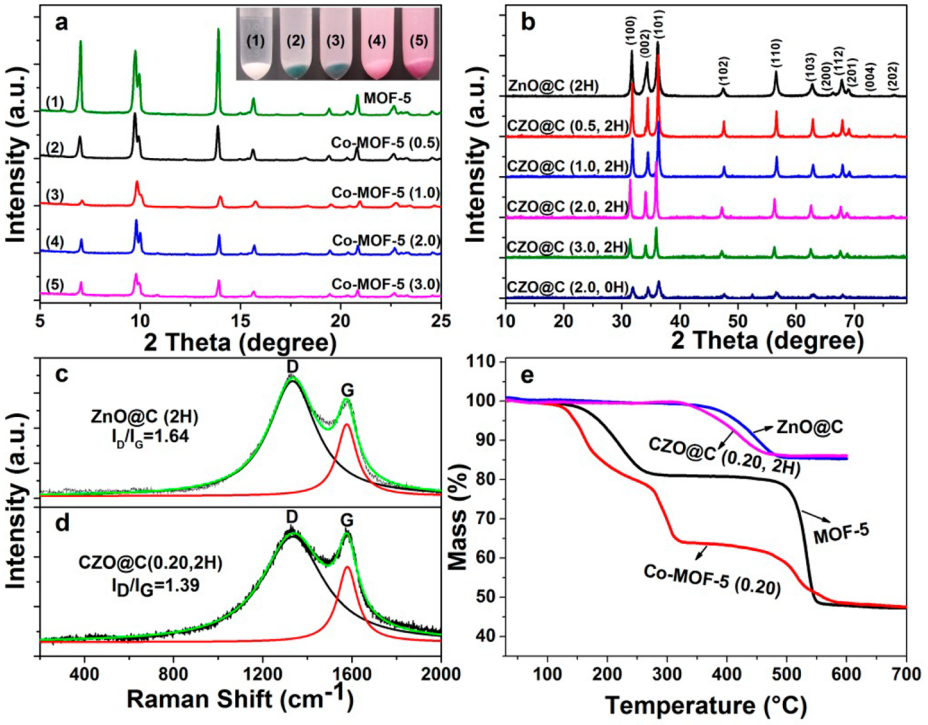

Figure 1. Digital photographs and XRD patterns of Co-MOF-5s: (a) XRD patterns of ZnO@C and CZO@C products; Raman shifts of the as-synthesized (b) ZnO@C (2H) and (c) CZO@C (2.0, 2H); TGA curves of (d) MOF-5 and (e) Co-MOF-5 (2.0) under a nitrogen atmosphere and CZO@C (2.0, 2H) and ZnO@C under an air atmosphere (10 °C min^{-1}).

washed repeatedly with ethanol and then dried in a vacuum oven at 60 °C.

The as-synthesized MOF-5 and Co-MOF-5 were heat-treated at 600 °C in a nitrogen atmosphere with a heating rate of 5 °C min^{-1}. After the target temperature was retained for 2 h, the materials were cooled to room temperature. The sample obtained by immediate cooling was also prepared as a contrast. The obtained ZnO@C and CZO@C composites were black composites, and they were named by the amount of cobalt nitrate and heating time. For example, CZO@C (2.0, 2H) means the doping amount of Co is 2.0% and the heating time at 600 °C is 2 h.

Material Characterization. Transmission electron microscopy (TEM; JEOL JEM-2100) and field-emission scanning electronic microscopy (SEM; JSM-6700F) were used to identify the morphological structure. X-ray diffraction (XRD) was carried out on a D8 Advance (Bruker) diffractometer using nickel-filtered Cu Kα radiation (λ = 0.154184 nm). The powder samples were scanned from 10° to 80° under the operation conditions of 40 kV and 40 mA. X-ray photoelectron spectroscopy (XPS; PHI 5700 ESCA) analysis was performed using monochromated Al Kα radiation ($h\nu$ = 1486.6 eV). Raman scattering measurements (Jobin Yvon Horiba HR800) were performed in a backscattering geometry at room temperature with a 514.5 nm line of an argon-ion laser. Thermal gravimetric analysis (TGA; NETZSCH STA 449F3) was applied to confirm the carbon content of the samples at a heating rate of 10 °C min^{-1} in an air atmosphere. Inductively coupled plasma mass spectrometry (ICP-MS; ELAN DRC-e; PerkinElmer SCIEX) was carried out to confirm the Co dopant. The samples were dissolved in concentrated nitric acid (Guarantee reagent; Sinopharm Chemical Reagent Co., Ltd.) and diluted with a 2% HNO_3 solution to 1000 mL, 1 mL of which was diluted to 100 mL by dideionized water. The Co/Zn atomic ratio was analyzed by ICP-MS according to eq 1:

$$\text{Co/Zn atom \%} = \frac{c_{Co}M_{Zn}}{c_{Zn}M_{Co}} \times 100\% \quad (1)$$

where c_{Co} and c_{Zn} represent the concentrations of Co^{2+} and Zn^{2+}, respectively, and M_{Co} and M_{Zn} represent the relative atomic mass of Co and Zn, respectively.

Electrochemical Measurements. For the electrochemical evaluation of ZnO@C and CZO@C, the test electrodes consisted of the active powder material (60 wt %), conductive carbon black (20 wt %) as a conductor, and poly(vinylidene fluoride) (20 wt %) dissolved in *N*-methylpyrrolidinone as a binder. Each component was mixed well to form a slurry that was coated on a copper foil substrate. Laboratory-made CR2032-type coin cells were assembled in an argon-filled glovebox using a Celgard 2400 as the separator, lithium foil as the counter and reference electrodes, and 1 M $LiPF_6$ in ethylene carbonate−dimethyl carbonate (1:1 volume) as the electrolyte. The coin cells were tested between 0.01 and 3.0 V (vs Li/Li^+) at a current density of 100 mA g^{-1} using a program-controlled battery test instrument (LAND CT2001A, China). The gravimetric capacity was calculated with respect to all active elements (ZnO and C). The electrochemical impedance spectrometry (EIS) spectra were conducted with a Solartron SI1287+SI1260 potentiometer at 25 °C with the frequency ranging from 100 kHz to 0.1 Hz.

3. RESULTS AND DISCUSSION

Digital photographs of Co-MOF-5s and XRD patterns of all products revealed the changes in color and the phase structures of as-synthesized MOF-5s, as shown in Figure 1a. The obtained MOF-5 exhibited peak positions similar to the previously reported experimental values of MOF-5s.[21,22] The doping of Co did not damage the framework structure of MOF-5.

It was obvious that all of the obtained ZnO composites had the same crystalline structure with intensity variations (Figure 1b). The diffraction patterns reflected the single-phase wurtzite structure of ZnO. There were no diffraction peaks of cobalt oxides or binary Zn/Co phases, indicating that Co was doped into the ZnO phase and a single phase was formed. The Co content and Co/Zn atomic ratio are shown in Table 1. The

Table 1. ICP-MS Results and Co/Zn Atomic Ratio of CZO@C Composites

sample name	m^a/mg	c_{Co}/μg L^{-1}	c_{Zn}/μg L^{-1}	Co/Zn atom %	Co wt %
CZO@C (0.5, 2H)	13.8	0.481	80.8	0.662	0.489
CZO@C (1.0, 2H)	14.8	1.08	91.6	1.30	0.963
CZO@C (2.0, 2H)	15.5	2.01	83.4	2.62	1.94
CZO@C (3.0, 2H)	15.2	2.79	71.7	4.17	3.11

$^a m$ = sample consumption in the digestion process.

main diffraction angles, lattice spaces, and crystal parameters of all CZO@C samples are shown in Table S1 in the Supporting Information (SI). The diffraction angles shifted to the high-angle region and the lattice spaces slightly decreased when the doping amounts were 0.5% and 1.0%, respectively. This might be because Co was substitutional impure in the ZnO phase,[23,24] owing to the smaller ion radius of Co^{2+} compared with that of Zn^{2+}. The doping form became interstitial when the doping amount reached 2.0%. The color changes (Figure 1a) of Co-MOF-5 (0.5 and 1.0) were obviously different from those of Co-MOF-5 (2.0 and 3.0), confirming the different doping forms. The peaks of CZO@C (2.0, 0H) were wider and weaker than those of other samples, indicating that the particle size of CZO@C (2.0, 0H) was much smaller than those of others according to the Scherrer equation, which was beneficial to the electrochemical performance.[16,25]

The Raman shifts of ZnO@C (2H) and CZO@C (2.0, 2H) are shown in Figure 1c,d. In these figures, two broad peaks at 1333.3 and 1581.1 cm^{-1} were obviously observed, which could be marked as the D and G bands of carbon, respectively.[26] The I_D/I_G ratios of the ZnO@C (2H) and CZO@C (2.0, 2H) materials were 1.64 and 1.39, respectively, indicating that the carbon in the CZO@C (2.0, 2H) composite had a higher graphitization degree.[27] A Co element catalyzed the carbon graphitization during pyrogenation of the organic compound.

Figure 1d showed the TGA curves of as-synthesized MOF and ZnO composites. The mass of MOFs was lost completely at a temperature of 550 °C under a nitrogen atmosphere, which was a little higher than the reported temperature owing to the quick heating rate.[10,21,28] The curve of Co-doped MOF was a little different from that of MOF-5 at a temperature of 300 °C, which was probably caused by the weight loss of $Co_2(OH)_2BDC$ or $Co(H_2O)_2BDC$.[29] The TGA curves of ZnO@C composites in an air atmosphere illustrated that the carbon content of the composites were 15% (Figure 1d). The mass loss occurred in the temperature range from 350 to 450 °C, which can be ascribed to the combustion of carbon in air.[30]

In order to examine the existence state of the elements in the as-synthesized CZO@C (2.0, 2H) and ZnO@C (2H), XPS measurements were carried out (Figure 2). Compared with the XPS survey spectrum of ZnO@C (2H), there was a weak peak at 780.5 eV, which proved the existence of a Co element in CZO@C (2.0, 2H) (Figure S1 in the SI). The binding energies of the Co $2p_{3/2}$ and Co $2p_{1/2}$ peaks were at 780.5 and 795.6 eV, respectively. The energy difference was 15.1 eV, which showed that the major existence state of the Co element was Co^{2+}.[31] The binding energies of the Zn $2p_{3/2}$ and Zn $2p_{1/2}$ peaks of ZnO@C (2H) were at 1020.7 and 1043.8 eV, indicating that the existence state of the Zn element was Zn^{2+}.[32,33] The relative peaks of CZO@C (2.0, 2H) were at 1021.1 and 1044.2 eV, a small positive shift of the bonding energy (Figure S2 in the SI), which was caused by Co doping. In the C 1s core level XPS spectrum (Figure 2a,b), the peaks at 284.4, 285.1, 286.8, and 289.1 eV belong to the bonds of C═C,[34,35] C−C,[36] C−O,[37]

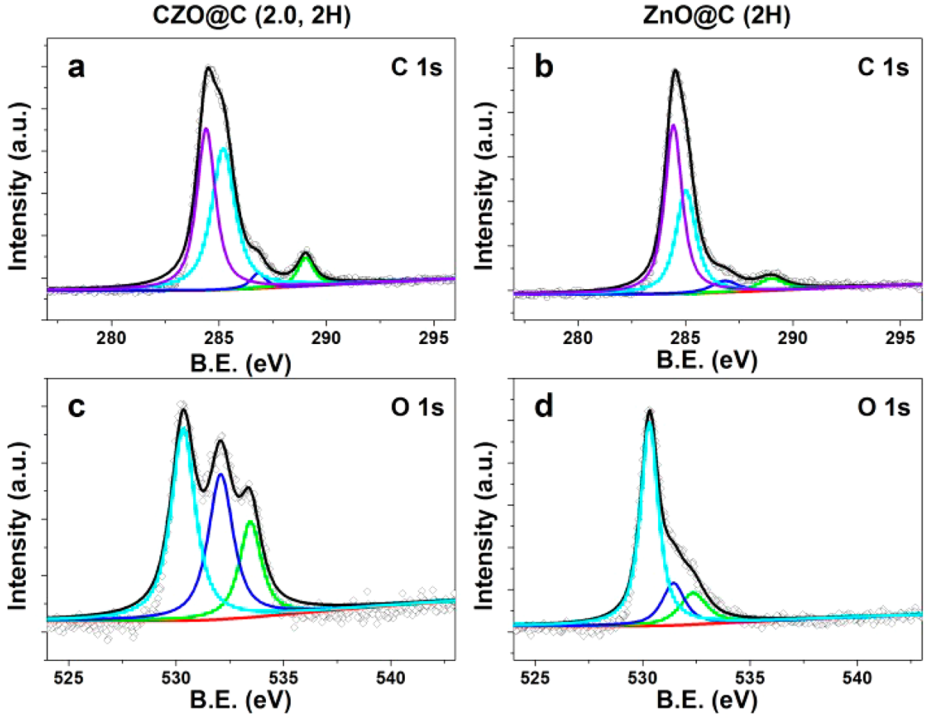

Figure 2. C 1s core level XPS profiles spectra of ZnO@C (2H) (a) and CZO@C (2.0, 2H) (b). O 1s core level XPS profiles spectra of ZnO@C (2H) (c) and CZO@C (2.0, 2H) (d).

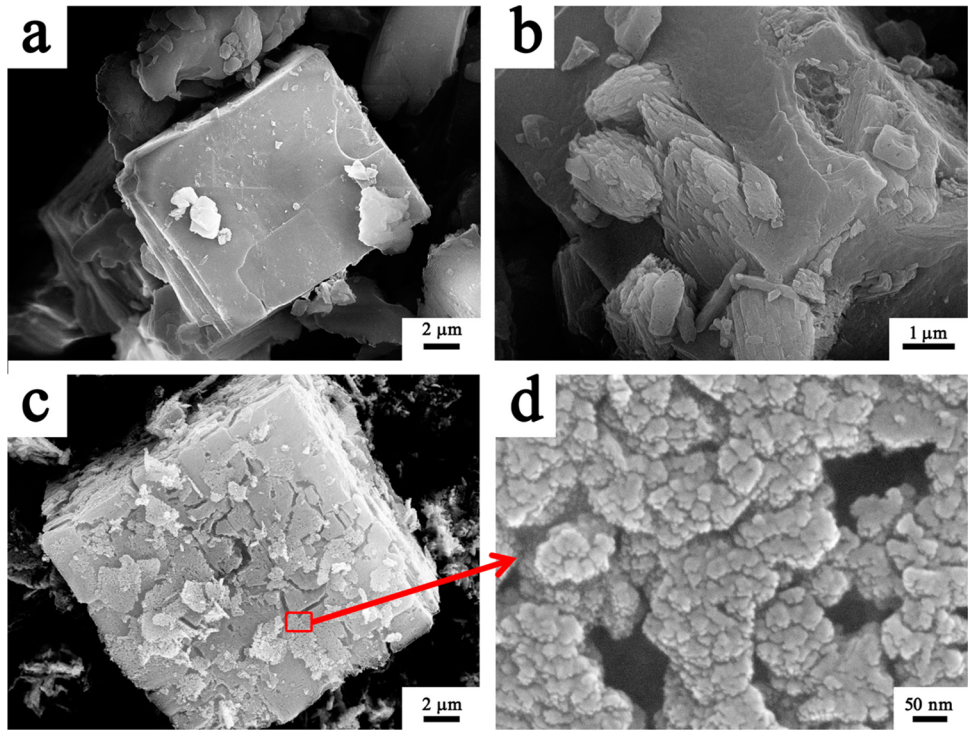

Figure 3. SEM images of MOF-5 (2.0) (a), MOF-5 (3.0) (b), and CZO@C (2.0, 2H) (c and d).

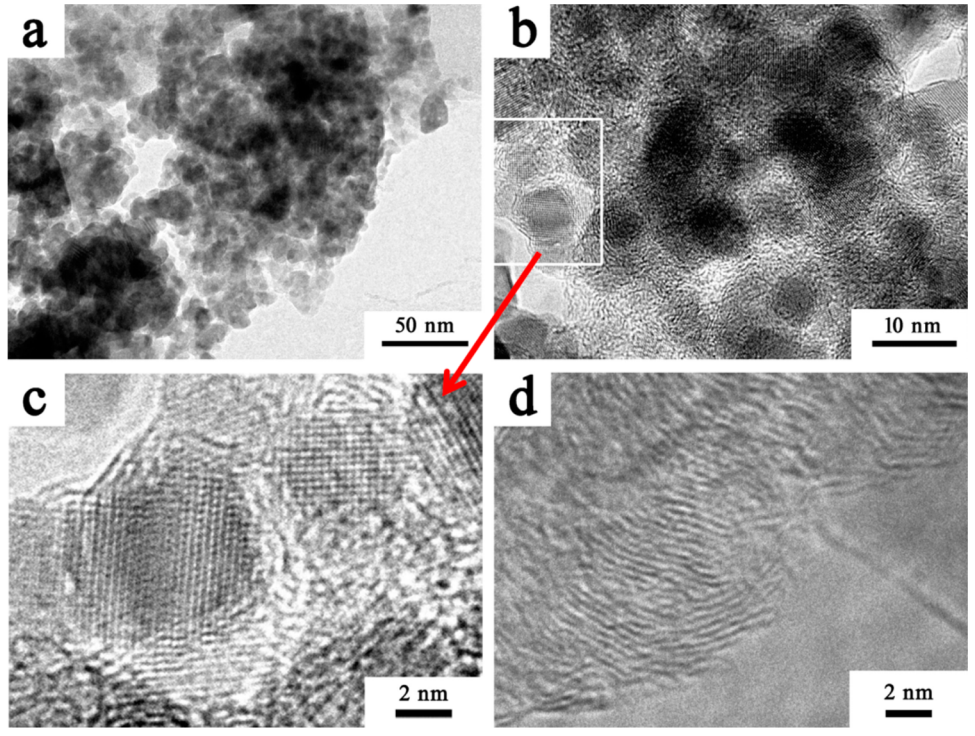

Figure 4. TEM (a and b) and HRTEM (c and d) images of CZO@C (2.0, 2H).

and O−C═O,[37] respectively. The peaks at 530.3, 532.2, and 533.4 eV in the O 1s core level XPS spectrum (Figure 2c,d) could be attributable to the bonds of metal−O,[38] O−C═O,[39] and C−O,[40] respectively. It was easy to confirm the formation of O-rich functional groups in the CZO@C (2.0, 2H) composites.[34] It was well-known that the O-rich functional groups possessed a quick Faradaic charge-transfer reactions (pseudocapacitance) as well as electrostatic charging.[41]

The as-synthesized Co-MOF-5s had a well-defined cubic morphology when the Co doping amount was less than 2.0% (Figure 3a). When the amount reached to 3.0%, some bamboo-shoot-like substances grew out (Figure 3b) and the cubic morphology was damaged by the water[42] that came from $Zn(NO_3)_2{\cdot}6H_2O$ and $Co(NO_3)_2{\cdot}6H_2O$. The substance might be some compounds of Co, such as $Co_2(OH)_2BDC$ or $Co(H_2O)_2BDC$.[29] The cubic structures of the samples were

dx.doi.org/10.1021/am5046873 | ACS Appl. Mater. Interfaces 2014, 6, 17067−17074

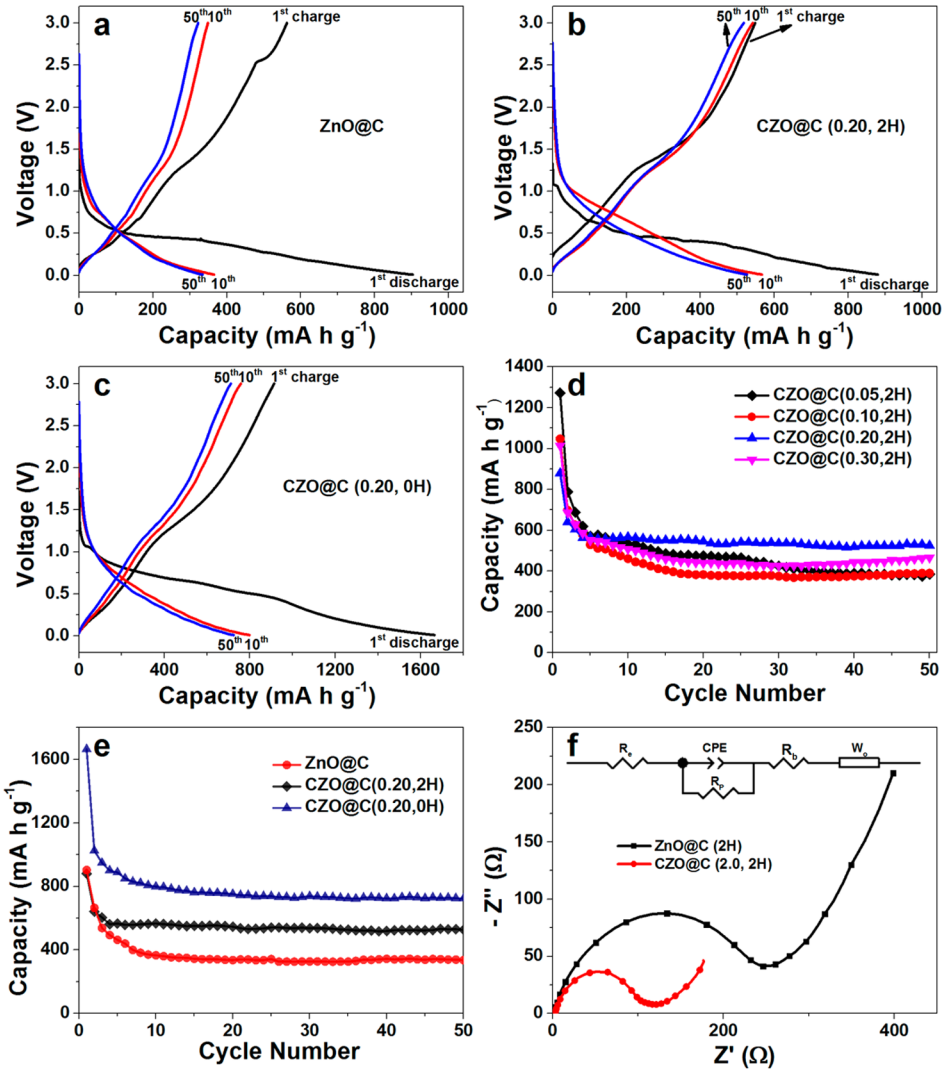

Figure 5. Charge−discharge curves of ZnO@C (a), CZO@C (2.0, 2H) (b), and CZO@C (2.0, 0H) (c); cycling performances of CZO@C (0.5, 2H), CZO@C (1.0, 2H), CZO@C (2.0, 2H), and CZO@C (3.0, 2H) (d); cycling performances of ZnO@C (2H), CZO@C (2.0, 2H), and CZO@C (2.0, 0H) (e); EIS of electrodes made by the ZnO composites and an equivalent circuit model after 50 cycles (f).

partly retained after thermal decomposition (Figure 3c). From the enlarged image (Figure 3d), it was found that the structure was assembled by small particles with a size of 20 nm at a higher amplification factor.

Figure 4 shows the TEM and high-resolution TEM (HRTEM) images of a CZO@C (2.0, 2H) composite. The composite existed in the forms of secondary particles (Figure 4a), and the primary particle sizes of CZO@C were about 20 nm, conforming to the SEM images. The Co-doped ZnO (CZO) particles were uniformly distributed in parent carbon with a size of less than 10 nm (Figure 4b). The interplanar spacings (Figure 4c) were 0.28 and 0.26 nm, which belonged to the (100) and (002) planes of ZnO. The values correspond to these calculations from the XRD pattern in Table S1 in the SI. The carbon was orderly arranged to a certain extent, and the diffraction fringe of carbon could be found in the HRTEM image (Figure 4d). The interplanar spacing was 0.34 nm, belonging to the (002) plane of graphite. This was a strong evidence that Co catalyzed the carbon atom transformation from sp^3 to sp^2 hybridization, which was in line with the XPS results.

The charge−discharge curves and cycling performances of ZnO@C and CZO@C composites are shown in Figure 5a−e. The reactions of CZO with lithium were similar to that of ZnO, including the reversible conversion metal oxide to nanosized metal and lithium oxide matrix and the alloying and dealloying processes of metal and lithium.[43] The reactions were as follows:

Discharge process:

$$CZO + 2Li^+ + 2e^- \rightarrow Zn + Co + Li_2O \quad (2)$$

$$Zn + Li^+ + e^- \rightarrow LiZn \quad (3)$$

$$Co + Li^+ + e^- \rightarrow LiCo \quad (4)$$

Charge process:

$$LiZn \rightarrow Zn + Li^+ + e^- \quad (5)$$

$$LiCo \rightarrow Co + Li^+ + e^- \quad (6)$$

$$Zn + Li_2O \rightarrow ZnO + 2Li^+ + 2e^- \quad (7)$$

$$Co + Li_2O \rightarrow CoO + 2Li^+ + 2e^- \quad (8)$$

dx.doi.org/10.1021/am5046873 | ACS Appl. Mater. Interfaces 2014, 6, 17067−17074

Table 2. Comparison of the Cycling Performances among ZnO-Based Anode Materials

electrode material	reversible capacity (mA h g^{-1})	cycle number	voltage (V)	rate (mA g^{-1})	ref
ZnO microrod	500	100	0–3.0	50	46
Au–ZnO flower	392	50	0.02–3.0	120	47
TiO_2-coated ZnO	447	30	0.3–3.0	50	44
flowerlike ZnO–CoO–C	438	50	0–2.5	494[a]	48
nickel-coated ZnO	490	30	0.02–3.0	80	45
ZnO–M/PC	653	100	0.1–3.0	100	30
ZnO/CNT	602	50	0–3.0	100	49
this work	725	50	0.01–3.0	100	

[a]The rate of 494 mA $g^{-1}$was 0.5C in ref 48.

The CZO@C composites exhibited an enhanced electrochemical performance compared with ZnO@C composites. The CZO@C (2.0, 2H) composites had a high discharge capacity of 525 mA h g^{-1} after 50 cycles, which was much higher than that of ZnO@C (335 mA h g^{-1} after 50 cycles). The CZO@C (2.0, 0H) had the best electrochemical performance of 725 mA h g^{-1} after 50 cycles among all of the samples, which might arise from the much smaller particle size of CZO@C (2.0, 0H) than those of the other samples. One advantage of smaller particle size was alleviating the capacity loss caused by volume expansion, and the other was facilitating the transportation of lithium ion and electron. Most importantly, it can enlarge the specific surface of the samples, leading to a larger contact area with the electrolyte. The initial discharge capacities of the three composites were 1663, 903, and 880 mA h g^{-1}, respectively. These characters became 1024, 665, and 640 mA h g^{-1} at the second cycle. These high irreversible capacities at the first cycle were caused by the formation of the solid electrolyte interphase layer on the surface of the electrode.[44] The capacity decay was quite large at the first five cycles. One reason was the morphological change during the formation of the Li_xZn alloys, and the other was the poor conductivity of ZnO.[45] The decay range of CZO@C was smaller than that of ZnO@C, which could be explained by the enhanced conductivity owing to Co doping. We have compared our work with some reported ZnO-based anode materials, and the results are summarized in Table 2, indicating that the CZO@C material exhibited a superior cycling performance compared with some reported results.

To further understand the improved lithium storage performance of the CZO@C composites, EIS experiments were carried out (Figure 5f). All of the Nyquist plots showed depressed separate semicircles in the middle- and high-frequency region and a straight line in the low-frequency region. The semicircles corresponded to charge-transfer resistances to lithium ions at the interface between the electrode and electrolyte (R_p) and the electronic resistivity of the active material and ionic conductivity in the electrode (R_b).[50] The straight line was assigned to the Warburg impedance (Wo) corresponding to the lithium diffusion process, and R_e represented the internal resistance of the test battery.[51,52] As shown in Figure 5f, CZO@C composites showed a distinctly smaller semicircle, indicating that it had lower charge-transfer impedances and electronic resistivity than that of ZnO@C composites, which was strong evidence that the Co doping could enhance the conductivity of ZnO.

4. CONCLUSIONS

An effective way to produce CZO nanoparticles coated with carbon (CZO@C composites) from Co-MOF-5 was reported in this paper. The doping of Co enhanced the conductivity of the samples substantially and promoted graphitization of carbon in the as-synthesized composites simultaneously. The synergetic effect is very important in the LIB field, as demonstrated here. When the material is used as an electrode material, CZO@C composites can reach a reversible capacity of 725 mA h g^{-1} up to the 50th cycle at a current density of 100 mA g^{-1}, which is higher than that of ZnO@C composites (335 mA h g^{-1}).

■ ASSOCIATED CONTENT

Supporting Information

Diffraction angles, interplanar spacing, and crystal parameters of all samples, XPS survey and profiles (Co 2p and Zn 2p core level) spectra of the as-synthesized ZnO@C (2H) and CZO@C (2.0, 2H) materials, and the electrochemistry performances of ZnO with Al doping and CZO prepared using a microwave-assisted combustion method, which are given as contrasts. This material is available free of charge via the Internet at http://pubs.acs.org.

■ AUTHOR INFORMATION

Corresponding Authors

*E-mail: yuehongyun@foxmail.com. Tel: (+86)-373-3326439. Fax: (+86)-373-3326439.

*E-mail: shutingyang@foxmail.com. Tel: (+86)-373-3326439. Fax: (+86)-373-3326439.

Notes

The authors declare no competing financial interest.

■ ACKNOWLEDGMENTS

This work was financially supported by Research Fund for the Doctoral Program of Higher Education of China (Grant qd12124), Major Science and Technology Projects in Henan Province (Grant 121100210500), and Key Project of Science and Technology of Henan Educational Committee (Grant 13A150518).

■ REFERENCES

(1) Li, S. L.; Xu, Q. Metal–Organic Frameworks as Platforms for Clean Energy. *Energy Environ. Sci.* **2013**, *6*, 1656–1683.

(2) Stock, N.; Biswas, S. Synthesis of Metal–Organic Frameworks (MOFs): Routes to Various MOF Topologies, Morphologies, and Composites. *Chem. Rev.* **2012**, *112*, 933–969.

(3) Xuan, W.; Zhu, C.; Liu, Y.; Cui, Y. Mesoporous Metal–Organic Framework Materials. *Chem. Soc. Rev.* **2012**, *41*, 1677–1695.

(4) Makal, T. A.; Li, J. R.; Lu, W.; Zhou, H. C. Methane storage in advanced porous materials. *Chem. Soc. Rev.* **2012**, *41*, 7761–7779.

(5) Jiang, H. L.; Tatsu, Y.; Lu, Z. H.; Xu, Q. Non-, Micro-, and Mesoporous Metal–Organic Framework Isomers: Reversible Trans-

formation, Fluorescence Sensing, and Large Molecule Separation. *J. Am. Chem. Soc.* **2010**, *132*, 5586−5587.
(6) Liu, J.; Chen, L.; Cui, H.; Zhang, J.; Zhang, L.; Su, C. Y. Applications of Metal−Organic Frameworks in Heterogeneous Supramolecular Catalysis. *Chem. Soc. Rev.* **2014**, *43*, 6011−6061.
(7) Morozan, A.; Jaouen, F. Metal Organic Frameworks for Electrochemical Applications. *Energy Environ. Sci.* **2012**, *5*, 9269−9290.
(8) Chaikittisilp, W.; Ariga, K.; Yamauchi, Y. A New Family of Carbon Materials: Synthesis of MOF-Derived Nanoporous Carbons and Their Promising Applications. *J. Mater. Chem. A* **2013**, *1*, 14−19.
(9) Yang, S. J.; Im, J. H.; Kim, T.; Lee, K.; Park, C. R. MOF-Derived ZnO and ZnO@C Composites with High Photocatalytic Activity and Adsorption Capacity. *J. Hazard. Mater.* **2011**, *186*, 376−382.
(10) Yang, S. J.; Nam, S.; Kim, T.; Im, J. H.; Jung, H.; Kang, J. H.; Wi, S.; Park, B.; Park, C. R. Preparation and Exceptional Lithium Anodic Performance of Porous Carbon-Coated ZnO Quantum Dots Derived from a Metal−Organic Framework. *J. Am. Chem. Soc.* **2013**, *135*, 7394−7397.
(11) Scrosati, B.; Hassoun, J.; Sun, Y. K. Lithium-Ion Batteries. A Look into the Future. *Energy Environ. Sci.* **2011**, *4*, 3287−3295.
(12) Goodenough, J. B.; Kim, Y. Challenges for Rechargeable Li Batteries. *Chem. Mater.* **2010**, *22*, 587−603.
(13) Fu, Z.-W.; Huang, F.; Zhang, Y.; Chu, Y.; Qin, Q.-Z. The Electrochemical Reaction of Zinc Oxide Thin Films with Lithium. *J. Electrochem. Soc.* **2003**, *150*, A714−A720.
(14) Wu, Z.-S.; Zhou, G.; Yin, L.-C.; Ren, W.; Li, F.; Cheng, H.-M. Graphene/metal oxide composite electrode materials for energy storage. *Nano Energy* **2012**, *1*, 107−131.
(15) Chen, J. J. Recent Progress in Advanced Materials for Lithium Ion Batteries. *Materials* **2013**, *6*, 156−183.
(16) Reddy, M. V.; Subba Rao, G. V.; Chowdari, B. V. Metal Oxides and Oxysalts as Anode Materials for Li Ion Batteries. *Chem. Rev.* **2013**, *113*, 53645−457.
(17) Li, H.; Wang, Z. X.; Chen, L. Q.; Huang, X. J. Research on Advanced Materials for Li-Ion Batteries. *Adv. Mater.* **2009**, *21*, 4593−4607.
(18) Chae, O. B.; Park, S.; Ryu, J. H.; Oh, S. M. Performance Improvement of Nano-Sized Zinc Oxide Electrode by Embedding in Carbon Matrix for Lithium-Ion Batteries. *J. Electrochem. Soc.* **2012**, *160*, A11−A14.
(19) Hwa, Y.; Sung, J. H.; Wang, B.; Park, C. M.; Sohn, H. J. Nanostructured Zn-Based Composite Anodes for Rechargeable Li-Ion Batteries. *J. Mater. Chem.* **2012**, *22*, 12767−12773.
(20) Guo, R.; Yue, W.; An, Y.; Ren, Y.; Yan, X. Graphene-Encapsulated Porous Carbon−ZnO Composites as High-Performance Anode Materials for Li-Ion Batteries. *Electrochim. Acta* **2014**, *135*, 161−167.
(21) Hafizovic, J.; Bjorgen, M.; Olsbye, U.; Dietzel, P. D. C.; Bordiga, S.; Prestipino, C.; Lamberti, C.; Lillerud, K. P. The Inconsistency in Adsorption Properties and Powder XRD Data of MOF-5 Is Rationalized by Framework Interpenetration and the Presence of Organic and Inorganic Species in the Nanocavities. *J. Am. Chem. Soc.* **2007**, *129*, 3612−3620.
(22) Saravanan, K.; Nagarathinam, M.; Balaya, P.; Vittal, J. J. Lithium Storage in a Metal Organic Framework with Diamondoid Topology—a Case Study on Metal Formates. *J. Mater. Chem.* **2010**, *20*, 8329−8335.
(23) Siddheswaran, R.; Mangalaraja, R. V.; Gomez, M. E.; Avila, R. E.; Jeyanthi, C. E. Room Temperature Ferromagnetism in Combustion Synthesized Nanocrystalline Co, Al Co-Doped ZnO. *J. Alloys Compd.* **2013**, *581*, 146−149.
(24) Wu, M.-S.; Chang, H.-W. Self-Assembly of NiO-Coated ZnO Nanorod Electrodes with Core−Shell Nanostructures as Anode Materials for Rechargeable Lithium-Ion Batteries. *J. Phys. Chem. C* **2013**, *117*, 2590−2599.
(25) Wang, H.; Dai, H. Strongly Coupled Inorganic-Nano-Carbon Hybrid Materials for Energy Storage. *Chem. Soc. Rev.* **2013**, *42*, 3088−3113.
(26) Zhu, Z. Q.; Wang, S. W.; Du, J.; Jin, Q.; Zhang, T. R.; Cheng, F. Y.; Chen, J. Ultrasmall Sn Nanoparticles Embedded in Nitrogen-Doped Porous Carbon as High-Performance Anode for Lithium-Ion Batteries. *Nano Lett.* **2014**, *14*, 153−157.
(27) Pol, V. G.; Wen, J. G.; Lau, K. C.; Callear, S.; Bowron, D. T.; Lin, C. K.; Deshmukh, S. A.; Sankaranarayanan, S.; Curtiss, L. A.; David, W. I. F.; Miller, D. J.; Thackeray, M. M. Probing the Evolution and Morphology of Hard Carbon Spheres. *Carbon* **2014**, *68*, 104−111.
(28) Kundu, T.; Sahoo, S. C.; Banerjee, R. Solid-State Thermolysis of Anion Induced Metal−Organic Frameworks to ZnO Microparticles with Predefined Morphologies: Facile Synthesis and Solar Cell Studies. *Cryst. Growth Des.* **2012**, *12*, 2572−2578.
(29) Kurmoo, M. Two Modifications of Layered Cobaltous Terephthalate: Crystal Structures and Magnetic Properties. *J. Solid State Chem.* **2001**, *159*, 343−351.
(30) Shen, X.; Mu, D.; Chen, S.; Wu, B.; Wu, F. Enhanced Electrochemical Performance of ZnO-Loaded/Porous Carbon Composite as Anode Materials for Lithium Ion Batteries. *ACS Appl. Mater. Interfaces* **2013**, *5*, 3118−3125.
(31) Yang, S. Y.; Lv, R. Q.; Wang, C. Z.; Liu, Y. Y.; Song, Z. Q. Structural and Magnetic Properties of Cobalt-Doped ZnO Thin Films on Sapphire (0001) Substrate Deposited by Pulsed Laser Deposition. *J. Alloys Compd.* **2013**, *579*, 628−632.
(32) Gao, S. Y.; Jia, X. X.; Yang, S. X.; Li, Z. D.; Jiang, K. Hierarchical Ag/ZnO Micro/Nanostructure: Green Synthesis and Enhanced Photocatalytic Performance. *J. Solid State Chem.* **2011**, *184*, 764−769.
(33) Hung, T. F.; Mohamed, S. G.; Shen, C. C.; Tsai, Y. Q.; Chang, W. S.; Liu, R. S. Mesoporous $ZnCo_2O_4$ Nanoflakes with Bifunctional Electrocatalytic Activities Toward Efficiencies of Rechargeable Lithium−Oxygen Batteries in Aprotic Media. *Nanoscale* **2013**, *5*, 12115−12119.
(34) Gao, S. Y.; Chen, Y. L.; Fan, H.; Wei, X. J.; Hu, C. G.; Wang, L. X.; Qu, L. T. A Green One-Arrow-Two-Hawks Strategy for Nitrogen-Doped Carbon Dots as Fluorescent Ink and Oxygen Reduction Electrocatalysts. *J. Mater. Chem. A* **2014**, *2*, 6320−6325.
(35) Gao, S. Y.; Geng, K. R. Facile Construction of Mn_3O_4 Nanorods Coated by a Layer of Nitrogen-Doped Carbon with High Activity for Oxygen Reduction Reaction. *Nano Energy* **2014**, *6*, 44−50.
(36) Zhuo, L. H.; Wu, Y. Q.; Ming, J.; Wang, L. Y.; Yu, Y. C.; Zhang, X. B.; Zhao, F. Y. Facile Synthesis of a Co_3O_4-Carbon Nanotube Composite and Its Superior Performance as an Anode Material for Li-Ion Batteries. *J. Mater. Chem. A* **2013**, *1*, 1141−1147.
(37) Poh, H. L.; Simek, P.; Sofer, Z.; Pumera, M. Sulfur-Doped Graphene via Thermal Exfoliation of Graphite Oxide in H_2S, SO_2, or CS_2 Gas. *ACS Nano* **2013**, *7*, 5262−5272.
(38) Borgel, V.; Gershinsky, G.; Hu, T.; Theivanayagam, M. G.; Aurbach, D. $LiMn_{0.8}Fe_{0.2}PO_4/Li_4Ti_5O_{12}$, a Possible Li-Ion Battery System for Load-Leveling Application. *J. Electrochem. Soc.* **2013**, *160*, A650−A657.
(39) McCafferty, E.; Wightman, J. Determination of the Concentration of Surface Hydroxyl Groups on Metal Oxide Films by a Quantitative XPS Method. *Surf. Interface Anal.* **1998**, *26*, 549−564.
(40) Li, B.; Wang, Y. Q.; Rong, H. B.; Wang, Y. T.; Liu, J. S.; Xing, L. D.; Xu, M. Q.; Li, W. S. A Novel Electrolyte with the Ability to Form a Solid Electrolyte Interface on the Anode and Cathode of a $LiMn_2O_4$/Graphite Battery. *J. Mater. Chem. A* **2013**, *1*, 12954−12961.
(41) Ruiz, V.; Blanco, C.; Raymundo-Pinero, E.; Khomenko, V.; Beguin, F.; Santamaria, R. Effects of Thermal Treatment of Activated Carbon on the Electrochemical Behaviour in Supercapacitors. *Electrochim. Acta* **2007**, *52*, 4969−4973.
(42) Greathouse, J. A.; Allendorf, M. D. The Interaction of Water with MOF-5 Simulated by Molecular Dynamics. *J. Am. Chem. Soc.* **2006**, *128*, 10678−10679.
(43) Dai, H.-Q.; Xu, H.; Zhou, Y.-N.; Lu, F.; Fu, Z.-W. Electrochemical Characteristics of Al_2O_3-Doped ZnO Films by Magnetron Sputtering. *J. Phys. Chem. C* **2012**, *116*, 1519−1525.
(44) Lee, J.-H.; Hon, M.-H.; Chung, Y.-W.; Leu, I.-C. The Effect of TiO_2 Coating on the Electrochemical Performance of ZnO Nanorod

as the Anode Material for Lithium-Ion Battery. *Appl. Phys. A: Mater. Sci. Process.* **2010**, *102*, 545−550.
(45) Zhang, C. Q.; Tu, J. P.; Yuan, Y. F.; Huang, X. H.; Chen, X. T.; Mao, F. Electrochemical Performances of Ni-Coated ZnO as an Anode Material for Lithium-Ion Batteries. *J. Electrochem. Soc.* **2007**, *154*, A65−A69.
(46) Huang, X. H.; Wu, J. B.; Lin, Y.; Guo, R. Q. ZnO Microrod Arrays Grown on Copper Substrates as Anode Materials for Lithium Ion Batteries. *Int. J. Electrochem. Sci.* **2012**, *7*, 6611−6621.
(47) Ahmad, M.; Yingying, S.; Nisar, A.; Sun, H.; Shen, W.; Wei, M.; Zhu, J. Synthesis of Hierarchical Flower-Like ZnO Nanostructures and Their Functionalization by Au Nanoparticles for Improved Photocatalytic and High Performance Li-Ion Battery Anodes. *J. Mater. Chem.* **2011**, *21*, 7723−7729.
(48) Wu, Z.; Qin, L.; Pan, Q. Fabrication and Electrochemical Behavior of Flower-Like ZnO−CoO−C Nanowall Arrays as Anodes for Lithium-Ion Batteries. *J. Alloys Compd.* **2011**, *509*, 9207−9213.
(49) Abbas, S. M.; Hussain, S. T.; Ali, S.; Ahmad, N.; Ali, N.; Abbas, S. Structure and Electrochemical Performance of ZnO/CNT Composite as Anode Material for Lithium-ion Batteries. *J. Mater. Sci.* **2013**, *48*, 5429−5436.
(50) Reddy, M. V.; Madhavi, S.; Rao, G. V. S.; Chowdari, B. V. R. Metal Oxyfluorides $TiOF_2$ and NbO_2F as Anodes for Li-Ion Batteries. *J. Power Sources* **2006**, *162*, 1312−1321.
(51) Chen, L.; Xu, H. Y.; Li, L.; Wu, F. F.; Yang, J.; Qian, Y. T. A Comparative Study of Lithium-Storage Performances of Hematite: Nanotubes vs. Nanorods. *J. Power Sources* **2014**, *245*, 429−435.
(52) Liu, B.; Zhao, X. Y.; Xiao, Y.; Cao, M. H. High-Surface-Area F-Doped Amorphous MoOx with High-Performance Lithium Storage Properties. *J. Mater. Chem. A* **2014**, *2*, 3338−3343.